THE JOURNAL OF PHYSICAL CHEMISTRY C

C: Physical Processes in Nanomaterials and Nanostructures

Direct Observation of Transition from Solid-State to Molecular-Like Optical Properties in Ultrasmall Silicon Carbide Nanoparticles

Dávid Beke, Anna Fucikova, Tibor Z. Jánosi, Gyula Károlyházy, Bálint Somogyi, Sándor Lenk, Olga Krafcsik, Zsolt Czigány, János Erostyák, Katalin Kamaras, Jan Valenta, and Adam Gali

J. Phys. Chem. C, **Just Accepted Manuscript** • DOI: 10.1021/acs.jpcc.8b07826 • Publication Date (Web): 25 Oct 2018

ACS Publications

is published by the American Chemical Society. 1155 Sixteenth Street N.W., Washington, DC 20036

Direct Observation of Transition from Solid-State to Molecular-Like Optical Properties in Ultrasmall Silicon Carbide Nanoparticles

David Beke[*†], Anna Fučíková[¥], Tibor Z. Jánosi[€‖], Gyula Károlyházy[†], Bálint Somogyi[†], Sándor Lenk[⊥], Olga Krafcsik[⊥], Zsolt Czigány[‡], János Erostyák[‖§], Katalin Kamarás[†], Jan Valenta[¥], and Adam Gali[*†⊥]

† Institute for Solid State Physics and Optics, Wigner Research Centre for Physics, Hungarian Academy of Sciences, Konkoly-Thege Miklós út 29-33., H-1121, Budapest, Hungary

¥ Charles University, Faculty of Mathematics and Physics, Department of Chemical Physics & Optics, Ke Karlovu 3, Prague 2, Czechia

€ MTA-PTE High-Field Terahertz Research Group, University of Pécs, Ifjúság útja 6., 7624 Pécs, Hungary

‖ University of Pécs, Szentágothai Research Center, Spectroscopy Research Group, Ifjúság útja 20., H-7624 Pécs, Hungary

§ University of Pécs, Institute of Physics, Ifjúság útja 6., H-7624 Pécs, Hungary

⊥ Department of Atomic Physics, Budapest University of Technology and Economics, Budafoki út 8., H-1111 Budapest, Hungary

‡ Institute for Technical Physics and Materials Science, Centre for Energy Research, Hungarian Academy of Sciences, Konkoly-Thege Miklós út 29-33., H-1121, Budapest, Hungary

*beke.david@wigner.mta.hu, gali.adam@wigner.mta.hu

ABSTRACT: We employ time-dependent photoluminescence (PL) and steady-state PL excitation (PLE) measurements to study the size dependent optical properties of ultrasmall silicon carbide (SiC) nanoparticles (NP). We find that the nature of the optical transition transforms from solid-state indirect gap to molecular-like as the diameter of spherical SiC NPs is reduced from 4-6 nm to 1-3 nm with a smooth transition in between. We deduce the radiative lifetimes of SiC NPs that are well supported by *ab initio* time-dependent density functional theory calculations on realistically large SiC NPs with realistic surface terminations, including the solvation effects.

Introduction

Silicon carbide (SiC) is a wide band gap indirect semiconductor known for its chemical resistance and hardness. It is used in a number of applications including abrasives[1], high-power electronics[2], and MEMS devices[3]. Its remarkable optical properties originating from bright optically active point defects can be utilized for quantum information processing[4,5]. Besides these properties, SiC is also a bioinert and hemocompatible material[6], and it is likely to keep these properties even on the nanoscale[7]. Indeed, SiC nanoparticles (NPs) are promising candidates for bioimaging and sensing as NPs smaller than 10 nm in size have enhanced luminescence properties[7–9], while their various surface moieties make them readily dispersible in polar solvents and biologically relevant media without the need of any surfactant or capping layer[10], which would increase their diameter. Despite these outstanding properties, the fundamental photophysics of SiC NPs is currently not as well understood as that of direct gap semiconductors such as CdSe. SiC NPs under 4 nm are easily prepared. However, such small nanoparticles show rather surface-dependent[11,12] than size-dependent optical properties[13] despite their semiconducting nature. Nevertheless, excitation dependent photoluminescence was demonstrated on SiC NPs solutions with broad size distribution[14] as a first experimental evidence of quantum confinement. However, that study did not describe the optical properties as a function of particle size.

It is hard to elucidate the quantum confinement effect for indirect semiconductors as the indirect transitions are forbidden and only the direct transitions are allowed in the first order. However, decreasing the nanoparticle size the selection rules can be changed and surface states cannot be neglected anymore. As a result, the observed spectrum may originate from various indistinguishable processes. The same difficulties with interpretation of the origin of luminescence have been found for silicon (Si) nanocrystals as well. Those nanocrystals are also made from an indirect band gap material. The difficulty of the analysis of the optical spectrum also arises from the limited synthetic capabilities for both materials. The Si NP surface is more reactive than a SiC NP, and it can be argued that

the surface effects in Si NPs have a stronger impact on the overall properties when compared with NPs made of direct band gap semiconductors[15,16]. Even though the interplay of quantum confinement with surface effects for Si NPs has seen considerable progress both theoretically and experimentally[17], it is still in the center of intense research[18–21]. Among surface states, for example, the manifestation of quantum confinement determines the optical properties which implies the possibility of indirect to direct transitions[22,23] that determine the size independent optical behavior of small Si NPs[24,25].

All of these phenomena may occur in SiC NPs, as SiC is a covalent indirect semiconductor akin to Si. On the other hand, SiC NPs prepared by various techniques exhibit broad particle size distributions making the experimental observation of such effects – surfaces and sizes – to be more difficult while no significant effort has been made to determine the optical properties of this material. SiC NPs are chemically stable that simplifies the evaluation of the system and helps the generalization of size and surface dependent properties for indirect semiconductor nanoparticles.

Here we describe the size dependent optical properties of SiC NPs with various surface terminations by analyzing observed spectroscopic data. The results are also supported by *ab initio* time-dependent density functional theory calculations. From the excitation emission matrices and size distributions we explore the impact of size reduction and surface states on the electronic structure and optoelectronic properties of SiC NPs. We recently showed that SiC NPs with diameter around twice the exciton Bohr radius can be prepared by the same stain etching method used for SiC NPs below 4 nm when the concentration of hexagonal inclusions in the bulk cubic SiC matrix is engineered[26]. The SiC NPs are in the size range of 3-6 nm and show red-shifted luminescence compared to smaller NPs reported earlier. The possibility to synthesize NPs with various sizes by the same method eliminates the necessity of the use of various techniques, and allows us to study the optical properties in a broad size range.

Methods

Cubic SiC powder was synthesized by bottom-up technique from its elements[27] (see the Supplementary Information for more details). SiC NPs were then fabricated from the SiC powder by the well described stain etching method.[24] Briefly, bulk cubic SiC is etched in a hot mixture of hydrofluoric acid and nitric acid solution. The thin porous layer, which is the result of the stain etching, was broken into SiC NPs by ultrasonication. Size distribution of SiC NPs was controlled through the density of hexagonal inclusions, or stacking faults (SF) in the cubic SiC powder as the applied acids are selective to the cubic polytype. We used aluminum as an additive to the mixture of silicon and carbon during SiC powder synthesis to vary the stacking fault concentration[26]. SiC NPs prepared from cubic SiC with low SF concentration are usually smaller than 4 nm. Increasing SF concentration increases the number of SiC NPs between 3-6 nm. In the case of the studied samples 5 m/m% Al is used to achieve ca. 15% SF concentration. Solutions that contain NPs between 1-4 nm are labeled as SiC-I while solutions that contain an additional fraction of 3-6 nm particles are labeled as SiC-II. Small particles were removed by using Pall Macrosep centrifuge filter with 1 kDa cutoff size to prepare unimodal 3-6 nm SiC NPs too (SiC-III).

As-prepared samples are carboxyl terminated[11,28]. Hydroxylated nanoparticles were obtained by reduction of SiC-I and SiC-II and are labeled as redSiC-I and redSiC-II, respectively. We used $NaBH_4$ to prepare hydroxylated samples. The method is described in Ref. 11. After the reduction, samples were filtered through an 1 kDa Pall Macrosep centrifuge filter and washed with high purity deionized water several times, in order to remove the added salts. The filtrate contains the aqueous solution of the aggregated NPs that were sonicated after washing to obtain single particles in solution.

Table 1 contains the studied samples and the corresponding properties.

Table 1. Sizes and surface termination of the studied SiC NPs solutions

Sample	Mean size (range)	Surface termination
SiC-I	2.8 nm (0.8 – 4.2 nm)	carboxyl
redSiC-I	2.8 nm (0.8 – 4.2 nm)	hydroxyl
SiC-II	4.1 nm (0.8 – 6.4 nm)	carboxyl
redSiC-II	4.1 nm (0.8 – 6.4 nm)	hydroxyl
SiC-III	4.8 nm (3.8 – 6.4 nm)	carboxyl

We used aqueous solutions for all the experiment. The particle concentration was kept in ca. 0.5 mg/ml.

High resolution transmission electron microscopy (HRTEM – JEOL JEM 3010) equipped with an electron energy loss spectrometer was used for size distribution characterization, material identification and elemental analysis. At least 300 particles were measured from several different TEM images for size distributions. Fast Fourier transform method was used to determine the lattice spacing of the nanoparticles and that was further confirmed by measuring the lattice distances of individual particles on TEM images. Attenuated total reflection infrared spectroscopy (ATR-IRIR – Bruker Tensor37 Fourier transform infrared spectrometer equipped with a zinc selenide horizontal multi-bounce attenuated total internal reflection accessory) was used for surface chemistry analysis. The chemical composition and the bonding state of the SiC sources were studied by X-ray photoelectron spectroscopy (XPS). The XPS spectra were obtained using an XR3E2 twin anode X-ray source (300W, VG Microtech) and a Clam2 truncated hemispherical electron energy analyzer (VG Microtech). The base pressure of the analysis chamber was around 4×10^{-9} mbar. Samples were analyzed using a MgKα (1253.6 eV) anode, without monochromatization. Peak fitting was carried out using CasaXPS software. Atomic absorption spectroscopy (AAS – Con-trAA-700 tandem spectrometer, Analytik Jena) and electron dispersive spectroscopy (EDS – Philips CM20 TEM instrument equipped with NORAN Voyager analyser) was used for precise chemical analysis[29]. UV-VIS spectoscopy (Ocean Optics, DH-2000-BAL light source and QE5000 spectrometer) and fluorescence spectroscopy (PL – Horiba Jobin-Yvon NanoLog FL3-2iHR spectrophotometer equipped with 450 W Xenon lamp for static measurements and NanoLED laser sources for time correlated single photon counting) were used to determine the optical properties of the NPs in the UV – VIS spectral range. All the absorption and fluorescence measurements were carried out in a 10 mm quartz cuvette (Hellma 110-QS). Excitation emission matrices (EEM) were measured using a xenon lamp for excitation, and double

monochromators at the excitation and the emission sides for wavelength selection. 0.2 nm slit sizes and 0.1 s integration times were applied during the measurements.

Size distribution was further analyzed with atomic force microscopy (AFM). A droplet of colloidal suspension of SiC NPs was placed on a Si wafer and then the excess material was removed after a few minutes. Size distributions of the SiC NPs were determined by AFM measurements, carried out by a Dimension Icon atomic force microscope (Bruker, Palaiseau, France) using tapping mode and Bruker MPP-11100-10 probe.

Time-correlated single photon counting (TCSPC) method was applied to obtain the fluorescence decay curves with time resolution of 55 ps. NanoLED-320,-455 pulsed LEDs served as excitation source, the emission wavelength maxima of the nanLEDs were 321 nm and 453 nm. The pulse duration was below 1.0 ns. The spectral ranges for Time Emission Matrix measurements varied with samples and with the excitation wave-length. This spectral range was 370-570 nm for SiC-I and 350-560 nm for redSiC-I, while 370-620 nm and 460-630 nm ranges were applied for SiC-II at the 321-nm and 453-nm excitation, respectively. The decay curves were recorded in these ranges with a spectral increment of 10 nm. The instrument response function was determined using Ludox as scattering medium. The real decay curves were extracted from the recorded data by deconvolution. The parameters of five-exponential decay model were calculated using a least-squares fitting technique for each emission wavelength. Global analysis with the five-exponential decay model using the same lifetime values for every single emission wavelength were achieved in order to create Decay Associated Spectra (DAS).

Quantum yield measurements were carried out with the Nanolog spectrophotometer in an F-3029 Quanta-φ integrating sphere, connected through an optical fiber interface.

Single nanoparticle luminescence spectroscopy was performed on samples formed by diluted suspensions drop-casted on cleaned Si wafers and dried. The micro-spectroscopy setup is based on an inverted microscope (Olympus IX-71) with a wide-field excitation in the epifluorescence configuration. Either 405-nm or 510-nm diode lasers were applied (beams are switchable using a folding mirror and the focal plane of excitation is shifted by a lens from the sample plane, in order to illuminate a broad spot of a sample and detect many emitting dots at once). The emitted signal is coupled to a 30-cm imaging spectrograph (Acton SpectraPro-2300i) with a back-thinned LN-cooled CCD camera (Princeton Instruments Spec-10:400B). Images are obtained using spectrograph gratings turned to zero-order. The area for spectral detection is selected by introducing a slit at the input image plane of a spectrometer and detected with a grating turned to a desired central wavelength position[30]. The spatial resolution of wide-field images is given by the diffraction limit to about 300 nm. The spectral sensitivity of the whole apparatus was calibrated using a radiation standard (45 W tungsten halogen lamp).

We also performed first-principles simulations for small sized SiC nanocrystals to validate the experimental results. The core of our model nanocrystal is built up from either 79 Si and 68 C atoms, or 68 Si and 79 C atoms, resulting in a spherical nanocrystal with a diameter of approximately 1.5 nm. For surface termination, we used the combination of the following surface groups (R)-OH, (R)-COOH, Si-O-Si, where R is Si or C. These results in spin singlet ground state configurations. The structures were relaxed utilizing density functional theory and the projector-augmented wave method[31] as implemented in the VASP code[32,33]. We utilized the PBE exchange-correlation functional[34], and applied 10 Å separation between the periodic images. The atoms were relaxed until all forces were smaller than 0.02 eV/Å. During the relaxation, solvation effects were taken into consideration utilizing the VASPsol solvation model[35]. The electronic structure, excitation energies and transition dipole moments were calculated utilizing time-dependent DFT (TD-DFT), using the Turbomole code.[36] For these calculations, the PBE0 hybrid-functional[37] was applied with DZP atomic basis-set, and the core electrons were taken into account with electron core potentials. Regarding the convergence in the Turbomole DZP basis set vs. VASP plane wave basis set, it provides relatively accurate Kohn-Sham energies for occupied and low energy unoccupied orbitals within about 0.1 eV by PBE functional. Previous test Turbomole calculations on the post relaxation from VASP geometries resulted in minor changes. We successfully applied this strategy on various systems previously.[11,38–41] For the TD-DFT calculations, solvation effects were considered using the COSMO model.[42]

The radiative lifetimes were calculated according to the Weisskopf-Wigner theory:

$$A = \frac{n\omega^3|\mu|^2}{3\pi\varepsilon_0\hbar c^3} = \frac{nE^3|\mu|^2}{3\pi\epsilon_0\hbar^4 c^3}, \quad (1)$$

where n is the refractive index, ω and μ are the energy and transition dipole moment of the first optical excitation and A is the decay rate of the excited state and the inverse of it is the radiative lifetime $\tau = 1/A$. The ultrasmall nanoparticles do not alter the refractive index of the medium, thus we applied the refractive index of unity and water for gas phase and in-water simulations, respectively.

We approximate the emission energy by the calculated optical gaps, i.e. the Stokes shift is neglected in our calculations. We also omitted the thermal averaging of radiative transition rates as it would require the calculation of higher energy excitations. This choice can be justified by the relatively large energy gaps between the first and second lowest energy excitation energies compared to the thermal energy ($\Delta E \approx 50$-100 meV vs. $k_B T \approx 26$ meV at room temperature) implying that our results are sufficiently accurate for the experimental spectra observed at room temperature.

Results and discussion

We already reported the size dependent emission properties of SiC NPs[26]. Even though the different size distribution is evident for the two samples, other factors than the size can be the reason for the red-shifted luminescence. A variety of measurements were carried out to determine the real source of the red shift. Fig. S2 shows the HRTEM images of SiC-I and SiC-II, respectively, both samples were crystalline with 2.4 nm lattice spacing corresponding to SiC. ATR-IRIR spectra show no differences in the surface terminations of the samples (Fig. S2 B). XPS, EDS, AAS were used for chemical analysis. We found that aluminum, applied for the regulation of stacking fault density in the SiC precursor, is not present in the SiC matrix or the final NPs. These measurements ruled out those differences in crystallinity, surface chemistry or doping would cause the distinction in the optical properties between SiC-I

and SiC-II (see the Supplemental Information (SI) for more details).

Fig. 1 shows the optical properties and size distributions of the studied samples. (The corresponding HRTEM images are shown in Fig. S2 in SI). Photoluminescence spectroscopy results (PL – Fig 1**A**) are in agreement with size distributions (Fig 1. B) showing unimodal and bimodal characteristics[43,44] for SiC-I and SiC-II samples, respectively. We also observe unimodal distribution after the small particles were filtered out from the SiC-II sample (Fig 1**C**, labeled as SiC-III). We conclude that only the size distribution shows consistent differences between SiC-I and SiC-II, therefore the red shift in the emission of SiC-II is caused by the increased size of nanoparticles in the SiC-II batch with respect to the SiC-I batch. Absorption spectra of SiC-I, SiC-II, redSiC-I, and redSiC-II samples (Fig. 1**D**) show broad shoulders very similar to the first transition bands of QDs with broad size distribution[45]. It is also shown that this shoulder is red-shifted for SiC-II compared to SiC-I. The shoulders are more visible after the subtraction of the exponential tail (Fig. 1**E**). These spectra show that the SiC-I sample contains one main absorption band while SiC-II contains an additional peak at longer wavelengths. The SiC-III sample, on the other hand, contains only the green band. This aspect of the absorption profile is similar to the measured size distribution and emission spectra confirming that shoulder positions in the absorption spectra are also size dependent. However, SiC is an indirect band gap semiconductor in its bulk form with nearly featureless absorption[13]. Even though direct-like transitions for Si NPs have been already reported[45] suggesting that these shoulders can be the results of quantum confinement, they can be connected to the surface moieties as well. Indeed, changing the surface termination also causes changes in the absorption spectra unraveling surface contribution to the absorption processes. After the reduction, absorbance is reduced, and the first maximum at 340 nm is shifted to 320 nm for both samples while the second peak of redSiC-II at 440 nm does not shift (Fig. 1**E**). We propose that the absorption peak centered at 290 nm is due to the presence of SiO_x related surface defects that are eliminated upon reduction[11,46] (see SI for more details).

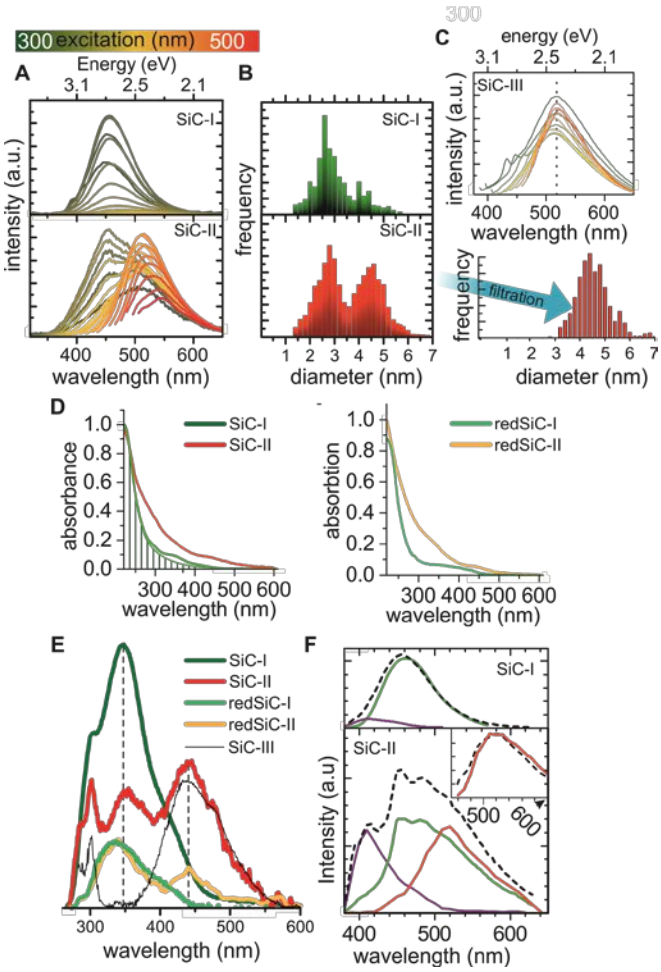

Figure 1.: (**A**) Photoluminescence emission spectra of SiC-I and SiC-II under different excitations. (**B**) Size distributions of SiC-I and SiC-II. (**C**) Photoluminescence emission spectra and size distribution of SiC-III under different excitations. (**D**) Absorption spectra of SiC-I, SiC-II, and redSiC-I, redSiC-II. Vertical lines highlight the exponential tail that is subtracted to construct figure **E**. (**E**) The extracted transition bands from the absorption spectra. (**F**) Decay associated spectra (DAS) of SiC-I and SiC-II under 321-nm excitation. The inset shows DAS of SiC-II under 453-nm excitation.

We showed that constructing DAS can help distinct overlapping emission pathways even in a colloid solution[11]. In Fig. 1**F**, the result of DAS for SiC-I and SiC-II samples can be seen. DAS shows two emission bands for SiC-I. These are the emission from SiC (the peak at ~450 nm) and an optically active center in the surface Si-O-Si bonds. In the case of SiC-II, we have three emitters. Two of them are similar to SiC-I, and an additional peak occurs at 530 nm.

As a result, absorption, steady state and time resolved emission measurements clearly show size dependent properties for SiC NPs in the size range of 1-6 nm. To further clarify the effects, we carried out single particle spectroscopy on the SiC-II sample. Representative spectra and the distribution of peak maxima can be seen in Fig. 2.

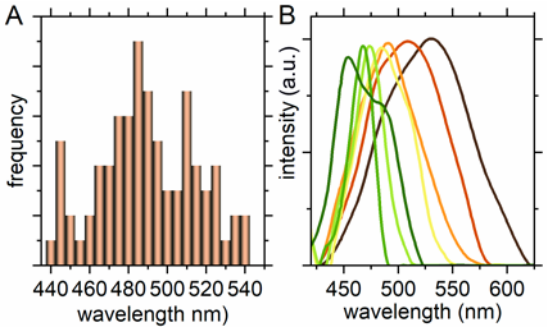

Figure 2.: (**A**) Distribution of peak maxima measured on 124 nanoparticles from the SiC-II sample. (**B**) Representative spectra from the 124 recorded emissions. Spectra were normalized and smoothed for the sake of visualization.

It should be noted that 405-nm excitation was used for single particle spectroscopy, therefore not all of the particles could be excited. Nevertheless, single particle spectroscopy reveals variations of spectra. When plotting the peak wavelength distribution (Fig. 2A), the result is very similar to the measured size distribution (Fig. 1B). It can be seen in Fig. 2B that some spectra have a distinguishable shoulder that can be explained with the aggregates as well.

Both the luminescence spectra of the examined solutions and single particle spectra suggest size dependent optical properties for SiC NPs. Because such dependency does not occur in ultrasmall particles, we monitored the threshold where the size dependent optical properties dissappear. To describe the dependencies, we compared the absorption and emission properties of the colloidal samples before and after surface modification. We recorded the excitation-emission matrices (EEM) of the samples, and we used the positions and the intensities of the PLE peak maxima at different excitation energies, together with the absorption spectra to study the effect of the size and the surface modifications. The position of PL peak maxima reflects the excitation dependent shift that is usually related to the quantum confinement, while PLE here is the position of the highest peak intensity as a function of excitation energy. We shall use the photon energy scale instead of wavelength in the rest of the paper. All curves are plotted as a function of excitation photon energy and can be found in Fig. 3.

If the colloid solution that contains NPs with different sizes is illuminated and the optical properties are size dependent, then different fractions are sampled by changing the excitation energy. If the excitation energy is low then only the largest particles are excited, and smaller particles stay dark – because smaller particles have larger band gap according to quantum confinement. When the excitation energy increases, the size of the smallest excited particle decreases and we sample larger and larger amounts of particles. At high excitation energy, all of the particles are excited. That results in a monotonous blue shift in the emission spectra. If the emission of SiC NPs is size dependent and there is no surface contribution, peak maxima of the carboxyl terminated and hydroxyl terminated samples should be at the same position, and they should shift with the excitation energy. Fig. 3 shows that this occurs for SiC-II and redSiC-II samples between 2.3-2.95-eV excitation energies and SiC-I samples between 2.7-2.95-eV excitation energies. We sample the largest particles in such an excitation range.

Above 2.95-eV excitation, the peak positions of the carboxyl and hydroxyl terminated samples are not identical anymore. The differences between peak positions for SiC-I and redSiC-I are increasing between 2.95-eV and 3.3.-3.5-eV excitation energies which implies an increasing contribution of surface states in the emission spectra. There are plateaus above 3.3-eV and 3.5-eV excitations for SiC-I and redSiC-I samples, respectively, showing size independent excitation that immediately implies size independent emission properties, even though the PLE maxima are at 3.87 eV and 3.95 eV for SiC-I and redSiC-I, respectively, suggesting that we still do not sample the mean sizes at 3.3-eV or 3.5-eV excitation that could be another explanation for the plateau.

The PLE and absorbance of such samples unravel the differences between the recombination processes as well. The emission intensities of SiC-I and redSiC-I decrease above 4.5-eV excitation energy. However, the PLE intensity of SiC-II and redSiC-II samples increases as the excitation energy increases just like the absorbance, implying that larger particles have continuous excitation spectra above the onset, similar to direct band gap semiconductor quantum dots[48,49], while small particles in SiC-I show narrow excitation spectra, similar to fluorescent organic molecules[50,51].

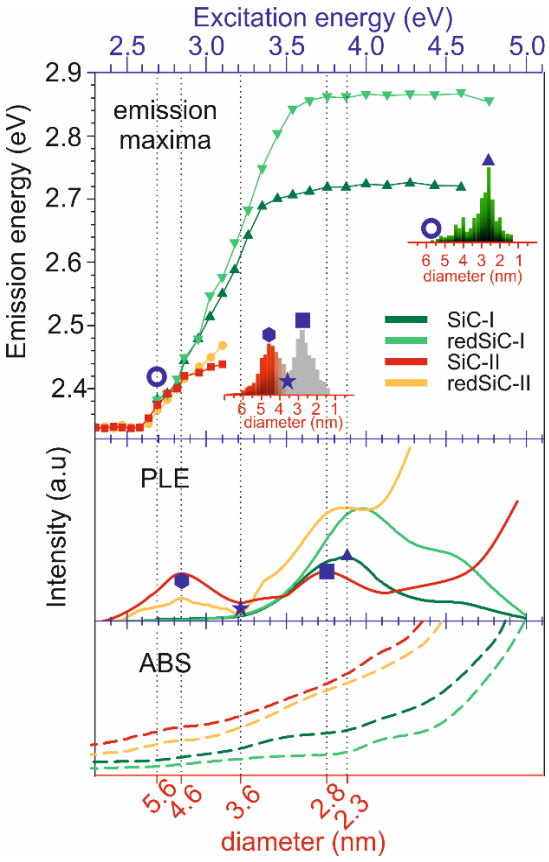

Figure 3.: Position of peak maxima as a function of excitation energy (scattered line), PLE (line) and absorption spectra (dashed line) of SiC-I (dark green), redSiC-I (light green), SiC-II (red) and redSiC-II (yellow).

All of these experimental observations demonstrate three distinct types of fluorescence from SiC NPs as the size of these particles changes. Large particles exhibit quantum

confinement while small particles show surface related, size independent emission, and there is a transition between the two.

These experimental data agree with the experimental results and theoretical calculations on Si NPs[17,19,52–54]. Indeed, it has been concluded that as the size of the particle decreases, contributions of the surface states increase flattening the enlargement of the band gap energy upon reduction of the crystal size, and surface states dominate the excitation and relaxation processes below 2 nm. A very similar effect was calculated for 4H-SiC NPs as well[55]. We also tried to estimate the relationship between the particle size and optical properties to give a comparable result for SiC NPs.

Both the absorption and the PLE spectra show size dependent behavior, however, it is likely that PLE consistently describes the size dependence because the presence of dark states influences the absorption spectra. We chose unique points in size distribution and PLE that we labeled in Fig. 3 with different symbols. SiC-II samples have two maxima and a minimum in the PLE spectra and the size distribution, and we used these three extrema. The SiC-I sample can be excited up to 2.7 eV (open blue circle in Fig 3) indicating that we excite here the largest particles present in the solution and it has only one PLE maximum that can be connected to its mean size. Then, we added more points from other samples with various size distributions from Refs. 11, 13, 55, 56, for the sake of accuracy (Fig. 4**A**). Indeed, the PLE maximum shifts with the mean size between 2.8 and 5 nm, and there is no shift below 2.8 nm.

The connection between the band gap energy and the particle size can be described with the effective mass approximation,

$$E(R) = E_g + \frac{a}{R^2} \qquad (2)$$

where *E(R)* is the size dependent band gap, *Eg* is the band gap of the bulk material, *a* is a constant, and *R* is the particle radius. We applied the effective mass approximation to the particles when there is a size dependent relation, allowing *Eg* to be a parameter in eq. 2, yielding 2.03 eV for the bulk band gap.

The effective mass approximation adequately describes the size dependence for particle sizes above 3.5 nm, however, most of the synthesized particles are smaller than that. As the surface contribution increases, the deviation from the effective mass theory also increases and below a certain size, the band gap is constant. Such behavior can be described by modification of eq. 2. with linear combination of a constant and the radius dependent function,

$$,E(R) = C - \left(E_g + \frac{a}{R^2}\right) e^{-\left(\frac{2R_d}{R}\right)^2} \qquad (3)$$

where the parameter *C* is the size independent excitation energy, and R_d is the particle size, above which surface states determine the emission spectra. Eq. 3 gives 3.87 eV for the *C* value, which is the measured PLE maximum for SiC-I samples and the corresponding particle size is 2.85 nm. Below the particle sizes of 2.85 nm, the quantum confinement effect vanishes and transforms into the size-independent molecular behavior (see Fig. 4A), and the size dependent semiconductor NP behavior between 2.8 and 3.75 nm. Eqs. (2) and (3) meet at the particle size of 3.75 nm, and for larger particles, the effective mass approximation is valid.

It can be seen in Fig 4**A** that the selected points from the two samples under consideration fit well to the curve demonstrating that the comparison of the mean sizes and the PLE maxima is sufficient to approximate the band gap of SiC NPs, if the mean particle size is larger than 3.75 nm.

The size above which the quantum confinement is not effective can also be estimated by extrapolation of the fitted curve. The emission of SiC-II NPs does not change for excitation photon energy below 2.6 eV and the emission maximum is at ~2.34 eV, which is the indirect band gap of 3C-SiC. Based on the extrapolation, we propose that quantum confinement disappears above the size of 5.8 nm. Larger particles have emission very close to the bulk material and do not change significantly anymore.

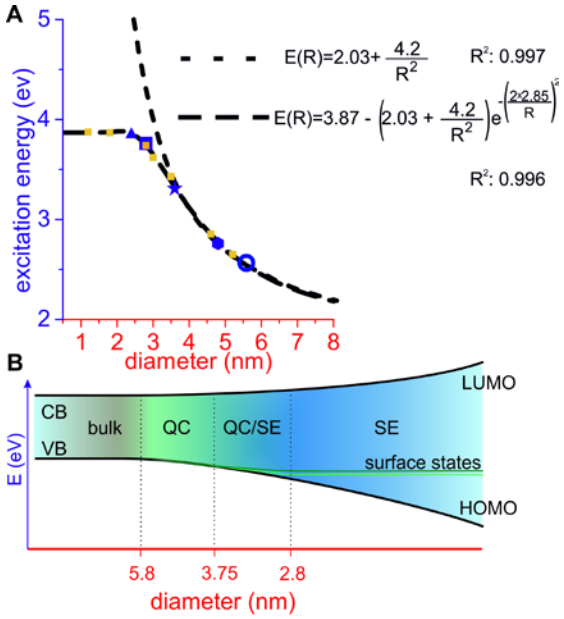

Figure 4.: (**A**) Size vs. excitation energy based on the PLEs and size distributions. Different symbols label reference points in Fig 2., while yellow symbols are from Refs. 11, 13, 55, 56. (**B**) Schematic representation of the band gap variation and properties change as a function of particle size, where QC stands for quantum confinement, SE for surface state related emission, VB for valence band energy, CB for conduction band energy, HOMO for the highest occupied molecular orbital and LUMO for the lowest unoccupied molecular orbital.

As we mentioned previously, PLE is not the only signal that reveals size dependency. Despite its indirect band gap, the absorption spectra of SiC NPs are not featureless. Size dependent shoulders in absorption spectra of Si NPs are often interpreted as a direct characteristic of the band gap and several reports give an account of such transition[22,23,45]. We further analyzed our data together with the results from density functional theory calculations, in order to study the change of indirect to direct transition upon reduction of the particle size.

Luminescence lifetime is a versatile tool for studying the recombination processes[23]. Indirect optical transitions are much less probable than the direct ones, because the participation of the third quasiparticle, the phonon, is required in order to fulfill the quasi-momentum conservation law. Therefore, the

radiative lifetime is an indicator of the band gap character. Radiative lifetime can be calculated from the measured quantum yield and luminescence lifetime.

$$QY = \frac{\tau}{\tau_r}, \qquad (4)$$

where QY is the quantum yield, τ is the measured lifetime and τ_r is the radiative lifetime. The measured decay times for SiC-I, redSiC-I and SiC-II with the calculated radiative lifetimes can be found in Table 2.

Table 2. External quantum yields and lifetimes. QY is the observed external quantum yield. Exc. is the excitation wavelength and Em. is the emission wavelength where quantum yield and lifetime were measured. τ is the observed luminescence lifetime whereas τ_r is the deduced radiative lifetime from the observed QY and τ. τ_r* is the calculated radiative lifetime from TD-DFT simulations in aqueous solution.

sample	QY (%)	τ (ns)	τ_r (ns)	Exc/Em (nm)	τ_{r*} (ns)
SiC-I	0.3	4.5	1500	300/450	1260
redSiC-I	0.4	8.1	2025	300/440	12270
SiC-II	1.2	6.1	505	440/530	

The microsecond radiative lifetimes indicate that the band gap of SiC NPs has indirect nature even at small sizes. We confirm the latter by our *ab initio* calculations on various SiC clusters (see Table S1). The calculated optical gaps, optical transition dipole moments and radiative lifetimes are listed in Table S2. We note that the radiative lifetimes simulated in water are predominantly shorter than the lifetimes simulated in vacuum that we tentatively attribute to the stronger confinement of the HOMO and LUMO orbitals in solvated molecules than in vacuum (gas phase). The radiative lifetimes simulated in water can be directly compared to experimental data that we show in Table 2. As we already published[11], the C-OH groups introduce the highest occupied molecular orbital (HOMO) in hydroxyl terminated SiC nanocrystal. We note that SiC nanocrystals with more C atoms than Si atoms generally exhibit a slightly higher gap (40 meV) compared to the opposite case. This small difference contributes to the inhomogeneous broadening in the observed photoluminescence spectrum. The substitution of Si-OH groups by Si-COOH groups on the surface leads to a redshift in the luminescence. According to the calculations, these surface related states contribute to the emission process and determine the radiation lifetime as well. In aqueous solution, the calculated lifetime for fully hydroxyl terminated nanocrystals is about 12 μs, while for carboxyl terminated ones, it is about 1-3 μs, in good agreement with the estimated radiative lifetime deduced from the experimental data..

We would like to mention here, that Eq.4 is strictly valid only for those emitters that are identical and there are no other are absorbing centers, which means that the external and internal quantum yields are the same. Also we neglected the possibility of intersystem-crossing that is reported for Si nanostructures[58] as the contribution of the triplet states to the emission is low at room temperature, and it is difficult to study this phenomena in a system with relatively broad size and surface distribution.

Tauc plots from the measured absorptions of redSiC-I and redSiC-II were also constructed (see Fig. S4 in SI). Even though this method is often used to characterize nanoparticle solutions, it is not suitable alone to determine the band gap and band structure[59]. Nevertheless an indirect fitting method gives reasonably good match for redSiC-II samples, while redSiC-I samples have very short linear part at both direct and indirect representation.

The lack of indirect to direct transition upon reduction of the size requires an alternative explanation on the observed shoulders in absorption spectra. Our results suggest that the shoulders are caused by surface states. The high energy shoulder shows the same shift during surface modification as the surface state originated DAS band. We also demonstrated that small SiC NPs have molecular like excitation spectra. Our calculations showed that the electronic states originated from the surface termination are connected to the HOMO of the nanocrystal. While there is no direct computational evidence but we think that this HOMO state is a subject of size dependence of the nanocrystals. We speculate that as the particle size increases and the band gap decreases, the conduction band and the valence band energies approximate the surface-related lowest unoccupied molecular orbital (LUMO) and HOMO energies, respectively, shrinking the differences between different surface states and forcing them to shift with the HOMO of the nanocrystal because of exchange interaction between the electrons. It means that the optical properties of SiC NPs, absorption and emission, are always influenced by surface states.

Conclusion

In conclusion, we showed that SiC NPs below 6 nm show size dependent optical properties. Bulk size effects dominate between 3.7-5.8 nm. Below 3.7 nm, the influence of surface states arises and becomes significant below 2.8 nm. With the increase of the relative number of surface atoms contributing to the surface states, the number of Si and C atoms contributing to the crystal core decreases rapidly which results in transformation from solid state to molecular behavior. Nevertheless, strength of optical transition is still relatively weak, in the order what is typical for indirect semiconductors.

SUPPORTING INFORMATION

Supporting Information accompanies this paper about TD-DFT results in detail, HRTEM images, XPS results, AAS results, ATR-IR spectra,, fitted curves on DAS spectra, Tauc plot.

ACKNOWLEDGMENT AG acknowledges the Hungarian NKFIH grant Nos. NVKP_16-1-2016-0043 and NN118161 as well as the National Quantum Technology Program (Grant No. 2017-1.2.1-NKP-2017-00001). DB acknowledges the TÁMOP-4.2.4.A/2-111/1-2012-00001 National Excellence Program, NTP-NFTÖ-18-B-0243, NTP-NFTÖ-16-0333, National Talent Programs. KK thanks for the support to Hungarian OTKA (NKFIH) project No. SNN 118012. Part of the work was supported by the V4+J Joint Research Project NaMSeN, (MSMT 8F15001) co-financed by the International Visegrad Fund. J. Erostyák and T. Z.

Jánosi thank the financial support of the Higher Education Institutional Excellence Program of the Ministry of Human Capacities in Hungary, within the framework of the 20765-3/2018/FEKUTSTRAT thematic program of the University of Pécs. The research was also supported by the

BME-Nanotechnology FIKP grant of the Ministry of Human Capacities in Hungary (BME FIKP-NAT).

REFERENCES

(1) Rosario, G. *Properties and Applications of Silicon Carbide*; Gerhardt, R., Ed.; InTech, 2011.

(2) Casady, J. B.; Johnson, R. W. Status of Silicon Carbide (SiC) as a Wide-Bandgap Semiconductor for High-Temperature Applications: A Review. *Solid. State. Electron.* **1996**, *39*, 1409–1422.

(3) Cheung, R. INTRODUCTION TO SILICON CARBIDE (SIC) MICROELECTROMECHANICAL SYSTEMS (MEMS). In *Silicon Carbide Microelectromechanical Systems for Harsh Environments*; PUBLISHED BY IMPERIAL COLLEGE PRESS AND DISTRIBUTED BY WORLD SCIENTIFIC PUBLISHING CO., 2006; pp 1–17.

(4) Castelletto, S.; Johnson, B. C.; Ivády, V.; Stavrias, N.; Umeda, T.; Gali, A.; Ohshima, T. A Silicon Carbide Room-Temperature Single-Photon Source. *Nat. Mater.* **2013**, *13*, 151–156.

(5) Castelletto, S.; Johnson, B.; Zachreson, C.; Beke, D.; Balogh, I.; Ohshima, T.; Aharonovich, I.; Gali, A. Room Temperature Quantum Emission from Cubic Silicon Carbide Nanoparticles. *ACS Nano* **2014**, *8*, 7938–7947.

(6) Schettini, N.; Jaroszeski, M. J.; West, L.; Saddow, S. E. Hemocompatibility Assessment of 3C-SiC for Cardiovascular Applications. In *Silicon Carbide Biotechnology*; Elsevier, 2012; pp 153–208.

(7) Beke, D.; Szekrényes, Z.; Pálfi, D.; Róna, G.; Balogh, I.; Maák, P. A.; Katona, G.; Czigány, Z.; Kamarás, K.; Rózsa, B.; et al. Silicon Carbide Quantum Dots for Bioimaging. *J. Mater. Res.* **2013**, *28*, 205–209.

(8) Botsoa, J.; Lysenko, V.; Géloën, a.; Marty, O.; Bluet, J. M.; Guillot, G. Application of 3C-SiC Quantum Dots for Living Cell Imaging. *Appl. Phys. Lett.* **2008**, *92*, 173902.

(9) Kharin, A.; Syshchyk, O.; Geloen, A.; Alekseev, S.; Rogov, A.; Lysenko, V.; Timoshenko, V. Carbon Fluoroxide Nanoparticles as Fluorescent Labels and Sonosensitizers for Theranostic Applications. *Sci. Technol. Adv. Mater.* **2015**, *16*, 044601.

(10) Fan, J.; Li, H.; Jiang, J.; So, L. K. Y.; Lam, Y. W.; Chu, P. K. 3C-SiC Nanocrystals as Fluorescent Biological Labels. *Small* **2008**, *4*, 1058–1062.

(11) Beke, D.; Jánosi, T. Z.; Somogyi, B.; Major, D. Á.; Szekrényes, Z.; Erostyák, J.; Kamarás, K.; Gali, A. Identification of Luminescence Centers in Molecular-Sized Silicon Carbide Nanocrystals. *J. Phys. Chem. C* **2016**, *120*, 685–691.

(12) Botsoa, J.; Bluet, J.; Lysenko, V.; Sfaxi, L.; Zakharko, Y.; Marty, O.; Guillot, G. Luminescence Mechanisms in 6H-SiC Nanocrystals. *Phys. Rev. B* **2009**, *80*, 1–6.

(13) Beke, D.; Szekrényes, Z.; Czigány, Z.; Kamarás, K.; Gali, Á. Dominant Luminescence Is Not Due to Quantum Confinement in Molecular-Sized Silicon Carbide Nanocrystals. *Nanoscale* **2015**, *7*, 10982–10988.

(14) Wu, X. L.; Fan, J. Y.; Qiu, T.; Yang, X.; Siu, G. G.; Chu, P. K. Experimental Evidence for the Quantum Confinement Effect in 3C-SiC Nanocrystallites. *Phys. Rev. Lett.* **2005**, *94*, 026102.

(15) Zhou, T.; Anderson, R. T.; Li, H.; Bell, J.; Yang, Y.; Gorman, B. P.; Pylypenko, S.; Lusk, M. T.; Sellinger, A. Bandgap Tuning of Silicon Quantum Dots by Surface Functionalization with Conjugated Organic Groups. *Nano Lett.* **2015**, *15*, 3657–3663.

(16) Romero, J. J.; Llansola-Portolés, M. J.; Dell'Arciprete, M. L.; Rodríguez, H. B.; Moore, A. L.; Gonzalez, M. C. Photoluminescent 1–2 Nm Sized Silicon Nanoparticles: A Surface-Dependent System. *Chem. Mater.* **2013**, *25*, 3488–3498.

(17) Wolkin, M.; Jorne, J.; Fauchet, P.; Allan, G.; Delerue, C. Electronic States and Luminescence in Porous Silicon Quantum Dots: The Role of Oxygen. *Phys. Rev. Lett.* **1999**, *82*, 197–200.

(18) Bürkle, M.; Lozac'h, M.; McDonald, C.; Mariotti, D.; Matsubara, K.; Švrček, V. Bandgap Engineering in OH-Functionalized Silicon Nanocrystals: Interplay between Surface Functionalization and Quantum Confinement. *Adv. Funct. Mater.* **2017**, *27*, 1701898.

(19) Puzder, A.; Williamson, A. J.; Grossman, J. C.; Galli, G. Surface Chemistry of Silicon Nanoclusters. *Phys. Rev. Lett.* **2002**, *88*, 097401.

(20) Clark, R. J.; Aghajamali, M.; Gonzalez, C. M.; Hadidi, L.; Islam, M. A.; Javadi, M.; Mobarok, M. H.; Purkait, T. K.; Robidillo, C. J. T.; Sinelnikov, R.; et al. From Hydrogen Silsesquioxane to Functionalized Silicon Nanocrystals. *Chem. Mater.* **2017**, *29*, 80–89.

(21) Gali, A.; Vörös, M.; Rocca, D.; Zimanyi, G. T.; Galli, G. High-Energy Excitations in Silicon Nanoparticles. *Nano Lett.* **2009**, *9*, 3780–3785.

(22) Poddubny, A. N.; Dohnalová, K. Direct Band Gap Silicon Quantum Dots Achieved via Electronegative Capping. *Phys. Rev. B* **2014**, *90*, 245439.

(23) Kůsová, K.; Hapala, P.; Valenta, J.; Jelínek, P.; Cibulka, O.; Ondič, L.; Pelant, I. Direct Bandgap Silicon: Tensile-Strained Silicon Nanocrystals. *Adv. Mater. Interfaces* **2014**, *1*, 1300042.

(24) de Boer, W. D. A. M.; Timmerman, D.; Dohnalová, K.; Yassievich, I. N.; Zhang, H.; Buma, W. J.; Gregorkiewicz, T. Red Spectral Shift and Enhanced Quantum Efficiency in Phonon-Free Photoluminescence from Silicon Nanocrystals. *Nat. Nanotechnol.* **2010**, *5*, 878–884.

(25) Luo, J.; Li, S.; Sychugov, I.; Pevere, F.; Linnros, J.; Zunger, A. Absence of Redshift in the Direct Bandgap of Silicon Nanocrystals with Reduced Size. *Nat. Nanotechnol.* **2017**, *12*, 930–932.

(26) Beke, D.; Károlyházy, G.; Czigány, Z.; Bortel, G.; Kamarás, K.; Gali, A. Harnessing No-Photon Exciton Generation Chemistry to Engineer Semiconductor Nanostructures. *Sci. Rep.* **2017**, *7*, 10599.

(27) Mukasyan, A. S.; Lin, Y. C.; Rogachev, A. S.; Moskovskikh, D. O. Direct Combustion Synthesis of Silicon Carbide Nanopowder from the Elements. *J. Am. Ceram. Soc.* **2013**, *96*, 111–117.

(28) Szekrényes, Z.; Somogyi, B.; Beke, D.; Károlyházy, G.; Balogh, I.; Kamarás, K.; Gali, A. Chemical Transformation of Carboxyl Groups on the Surface of Silicon Carbide Quantum Dots. *J. Phys. Chem. C* **2014**, *118*, 19995–20001.

(29) Dravecz, G.; Bencs, L.; Beke, D.; Gali, A. Determination of Silicon and Aluminum in Silicon Carbide Nanocrystals by High-Resolution Continuum Source Graphite Furnace Atomic Absorption Spectrometry. *Talanta* **2016**, *147*, 271–275.

(30) Sychugov, I.; Valenta, J.; Linnros, J. Probing Silicon Quantum Dots by Single-Dot Techniques. *Nanotechnology* **2017**, *28*, 072002.

(31) Blöchl, P. E. Projector Augmented-Wave Method. *Phys. Rev. B* **1994**, *50*, 17953–17979.

(32) Kresse, G.; Hafner, J. Ab Initio Molecular Dynamics for Liquid Metals. *Phys. Rev. B* **1993**, *47*, 558–561.

(33) Kresse, G.; Furthmüller, J. Efficient Iterative Schemes for Ab Initio Total-Energy Calculations Using a Plane-Wave Basis Set. *Phys. Rev. B* **1996**, *54*, 11169–11186.

(34) Perdew, J. P.; Burke, K.; Ernzerhof, M. Generalized Gradient Approximation Made Simple. *Phys. Rev. Lett.* **1996**, *77*, 3865–3868.

(35) Mathew, K.; Sundararaman, R.; Letchworth-Weaver, K.; Arias, T. A.; Hennig, R. G. Implicit Solvation Model for Density-Functional Study of Nanocrystal Surfaces and Reaction Pathways. *J. Chem. Phys.* **2014**, *140*, 084106.

(36) Ahlrichs, R.; Bär, M.; Häser, M.; Horn, H.; Kölmel, C. Electronic Structure Calculations on Workstation Computers: The Program

System Turbomole. *Chem. Phys. Lett.* **1989**, *162*, 165–169.

(37) Perdew, J. P.; Ernzerhof, M.; Burke, K. Rationale for Mixing Exact Exchange with Density Functional Approximations. *J. Chem. Phys.* **1996**, *105*, 9982–9985.

(38) Vlasov, I. I.; Shiryaev, A. A.; Rendler, T.; Steinert, S.; Lee, S.-Y.; Antonov, D.; Vörös, M.; Jelezko, F.; Fisenko, A. V; Semjonova, L. F.; et al. Molecular-Sized Fluorescent Nanodiamonds. *Nat. Nanotechnol.* **2014**, *9*, 54–58.

(39) Gali, A. Time-Dependent Density Functional Study on the Excitation Spectrum of Point Defects in Semiconductors. *Phys. status solidi* **2011**, *248*, 1337–1346.

(40) Vörös, M.; Deák, P.; Frauenheim, T.; Gali, A.; Vörös, M.; Deák, P. The Absorption Spectrum of Hydrogenated Silicon Carbide Nanocrystals from Ab Initio Calculations. *Appl. Phys. Lett.* **2010**, *96*, 051909.

(41) Vörös, M.; Deák, P.; Frauenheim, T.; Gali, A. The Absorption of Oxygenated Silicon Carbide Nanoparticles. *J. Chem. Phys.* **2010**, *133*, 064705.

(42) Klamt, A.; Schüürmann, G. COSMO: A New Approach to Dielectric Screening in Solvents with Explicit Expressions for the Screening Energy and Its Gradient. *J. Chem. Soc., Perkin Trans. 2* **1993**, No. 5, 799–805.

(43) Zhou, Y.; Zhang, J.; Ning, Y.; Zeng, Y.; Zhang, J.; Zhang, X.; Qin, L.; Wang, L. Bimodal-Sized Quantum Dots for Broad Spectral Bandwidth Emitter. *Opt. Express* **2015**, *23*, 32230.

(44) Souaf, M.; Baira, M.; Nasr, O.; Alouane, M. H. H.; Maaref, H.; Sfaxi, L.; Ilahi, B. Investigation of the InAs/GaAs Quantum Dots' Size: Dependence on the Strain Reducing Layer's Position. *Materials (Basel).* **2015**, *8*, 4699–4709.

(45) Dohnalová, K.; Poddubny, A. N.; Prokofiev, A. A.; de Boer, W. D.; Umesh, C. P.; Paulusse, J. M.; Zuilhof, H.; Gregorkiewicz, T. Surface Brightens up Si Quantum Dots: Direct Bandgap-like Size-Tunable Emission. *Light Sci. Appl.* **2013**, *2*, e47–e47.

(46) Pankratov, V.; Osinniy, V.; Kotlov, A.; Nylandsted Larsen, A.; Bech Nielsen, B. Si Nanocrystals Embedded in SiO2 : Optical Studies in the Vacuum Ultraviolet Range. *Phys. Rev. B* **2011**, *83*, 045308.

(47) Somogyi, B. First Principles Study of Silicon Carbide Nanocrystals, Budapest University of Technology and Economics, 2017.

(48) Mukherjee, A.; Ghosh, S. Optimum Excitation Photon Energy for CdSe–ZnS Core–shell Quantum Dot Based Luminescence Imaging. *J. Phys. D. Appl. Phys.* **2012**, *45*, 195103.

(49) Bing-Can, L.; Xue-Qin, P.; Qiang, T.; Zheng-Long, W. PLE Spectra Analysis of the Sub-Structure in the Absorption Spectra of CdSeS Quantum Dots. *Chinese Phys.* **2006**, *15*, 1067–1070.

(50) Kairdolf, B. A.; Smith, A. M.; Stokes, T. H.; Wang, M. D.; Young, A. N.; Nie, S. Semiconductor Quantum Dots for Bioimaging and Biodiagnostic Applications. *Annu. Rev. Anal. Chem. (Palo Alto. Calif).* **2013**, *6*, 143–162.

(51) Yu, J.; Xu, C.; Tian, Z.; Lin, Y.; Shi, Z. Facilely Synthesized N-Doped Carbon Quantum Dots with High Fluorescent Yield for Sensing Fe^{3+}. *New J. Chem.* **2016**, *40*, 2083–2088.

(52) Valenta, J.; Fucikova, A.; Vácha, F.; Adamec, F.; Humpolíčková, J.; Hof, M.; Pelant, I.; Kůsová, K.; Dohnalová, K.; Linnros, J. Light-Emission Performance of Silicon Nanocrystals Deduced from Single Quantum Dot Spectroscopy. *Adv. Funct. Mater.* **2008**, *18*, 2666–2672.

(53) Hori, Y.; Kano, S.; Sugimoto, H.; Imakita, K.; Fujii, M. Size-Dependence of Acceptor and Donor Levels of Boron and Phosphorus Codoped Colloidal Silicon Nanocrystals. *Nano Lett.* **2016**, *16*, 2615–2620.

(54) Li, H.; Wu, Z.; Zhou, T.; Sellinger, A.; Lusk, M. T. Tailoring the Optical Gap of Silicon Quantum Dots without Changing Their Size. *Phys. Chem. Chem. Phys.* **2014**, *16*, 19275–19281.

(55) Rashid, M.; Tiwari, A. K.; Goss, J. P.; Rayson, M. J.; Briddon, P. R.; Horsfall, A. B. Surface-State Dependent Optical Properties of OH-, F-, and H-Terminated 4H-SiC Quantum Dots. *Phys. Chem. Chem. Phys.* **2016**, *18*, 21676–21685.

(56) Beke, D.; Szekrényes, Z.; Balogh, I.; Veres, M.; Fazakas, É.; Varga, L. K.; Kamarás, K.; Czigány, Z.; Gali, A. Characterization of Luminescent Silicon Carbide Nanocrystals Prepared by Reactive Bonding and Subsequent Wet Chemical Etching. *Appl. Phys. Lett.* **2011**, *99*, 213108.

(57) Beke, D.; Szekrényes, Z.; Balogh, I.; Czigány, Z.; Kamarás, K.; Gali, A. Preparation of Small Silicon Carbide Quantum Dots by Wet Chemical Etching. *J. Mater. Res.* **2013**, *28*, 44–49.

(58) Kovalev, D.; Heckler, H.; Polisski, G.; Koch, F. Optical Properties of Si Nanocrystals. **1999**, *871*, 871–932.

(59) Feng, Y.; Lin, S.; Huang, S.; Shrestha, S.; Conibeer, G. Can Tauc Plot Extrapolation Be Used for Direct-Band-Gap Semiconductor Nanocrystals? *J. Appl. Phys.* **2015**, *117*, 125701.

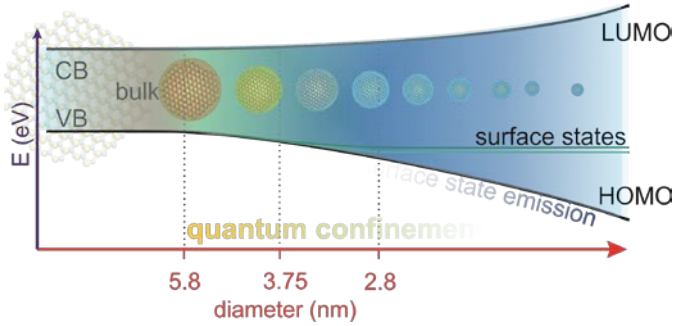
LUMO
CB
bulk
VB
surface states
HOMO
E (eV)
quantum confinement
5.8
3.75
2.8
diameter (nm)

TOC Graphic